Characterization of the turbulent flame front surface in SI engines during SI operation to identify CAI and abnormal combustion

Vicente Macián, J. Javier López, Jaime Martín and Jorge Valero-Marco

Abstract

The combustion diagnostics and subsequent analysis are somehow standardized tools based on the estimation of the Heat Release Law (HRL). From this estimation, the different combustion parameters can be obtained: combustion phasing and duration, heat release rate, etc. This analysis might be usually enough to study traditional Spark Ignition (SI) engines. However, with the new upcoming SI engines, this is probably not the case anymore, since different combustion modes can be operated in the same engine, as for instance a combination of SI and Controlled Auto-Ignition (CAI) combustion modes. When different combustion modes are combined, it seems interesting to study in more depth the HRL, trying to get more data and to study the differences among the diverse combustion modes. For this end, a methodology to go deeper in the study of the HRL is proposed in this work, consisting mainly in quantifying and taking into account the most relevant influencing parameters: the fuel properties (mainly its Lower Heating Value), the in-cylinder oxygen content, the density of the burned and unburned zones, the laminar combustion speed and the turbulence effect. With the proposed methodology, a standard SI combustion, developed by a flame front, can be characterized, allowing to predict, at any given operating point, which the combustion development would be assuming it to be developed by a flame front. Subsequently, this SI combustion prediction can be compared to the one obtained experimentally, making it possible to identify and analyze abnormal combustion phenomena, as well as to study the differences between a combustion developed by a flame front (SI) and by auto-ignition (CAI). Derived from this work, an alternative equation to experimentally characterize the laminar combustion velocity has also been proposed, in order to improve its applicability in a wider range of Fuel/Air ratios and dilution degrees.

Keywords

HRL, CAI, SI, combustion analysis, combustion speed

Introduction

The combustion diagnostics is a key tool to obtain precious data from the combustion process occurred during any engine test. This process represents the way how the energy is introduced in the engine, which is later partly recovered at the power stroke. Therefore, the way in which combustion is developed plays an important role on the

Corresponding author:

J. Javier López

CMT-Motores Térmicos, Universitat Politècnica de València, Spain

engine performance. The most extended way to analyze the combustion is the estimation of the heat release law (HRL), which represents the way in which the fuel is burnt. In the literature, two main ways to estimate the HRL can be found: the "burning rate analysis", and the "heat release analysis"[1;2].

- The burning rate analysis comes from SI engines, in which two regions can be clearly differentiated during the combustion development: the burned and the unburned regions. The estimation of this parameter is based on simplified models to approximate the thermodynamic evolution of the cylinder charge, and one of the most widespread models is that of Rassweiler and Withrow[3]. By analogy with a constant volume combustion, the authors link the pressure increment with the evolution of the burned fraction.

- The heat release analysis is based on the application of an energy balance to the combustion chamber, based on the first law of thermodynamics. All the variables of this balance are considered: internal energy, expansion work, heat flow to the walls and enthalpy of the combustion chamber incoming and out-coming mass flows. Usually the most important parameters for this estimation are the internal energy and the expansion work, and the rest of the variables can be simplified or even neglected. According to Heywood[1], it is usual to differentiate between two ways to estimate this HRL:

    – The first one takes into account the heat losses to the cylinder walls, and consequently the chemical energy released from the fuel can be estimated*. This estimated HRL is known in the literature as the gross heat release[1;2;4;5].

    – The second way does not consider any heat loss for the estimation of the HRL. By this way, the obtained HRL is known as the net heat release[1;6;7].

From this law, different parameters, such as its derivative, the Heat Release Rate (HRR), and other related parameters, such as the combustion phasing, are obtained. This HRL depends on multiple factors affecting the combustion development: the fuel used, the mass trapped inside the cylinder, the in-cylinder charge temperature and pressure, the Fuel/Air ratio, the turbulence effect, the mixture dilution, the combustion chamber design and the mixture homogenization[4]. All these variables affect the performance of the combustion process, and their characterization can help to perform a more complete combustion analysis.

Nowadays, different combustion modes are under study in SI engines[8]. The most usual and extended mode is the SI combustion under stoichiometric conditions, which has been investigated since long time ago. This combustion process is based on a turbulent flame propagation, which is a function of the estimated laminar combustion speed and the modification of this speed caused by the turbulence inside the combustion chamber[9]. Many authors, as e.g. Metghalchi and Keck[10], and Rhodes and Keck[11], have obtained empirical correlations for the estimation of the laminar combustion speed as a function of temperature, pressure and Fuel/Air equivalence ratio, for different fuels used in SI engines.

However, other combustion modes, like SI combustion under lean conditions (SI lean)[12;13] or CAI combustion (Controlled Auto-Ignition)[14;15] start to be implemented in current engines. These combustion modes operate in a different way: the SI lean is based on the propagation of a turbulent flame front, but with a Fuel/Air ratio of the mixture that is inside the lean range, whereas the CAI combustion takes place by autoignition of the different regions along the whole combustion chamber. Therefore, it is worth to discuss

Camino de Vera, s/n. 46022 Valencia, SPAIN

Tel: +34 963 879 232. Fax: +34 963 877 659

Email: jolosan3@mot.upv.es

*This is the chosen methodology for the HRL estimations all along this work.

how the combustion diagnostic and analysis are performed for these different combustion modes.

The ways to characterize each combustion mode are very different, since (as stated before) they are governed by clearly different mechanisms. For this reason, it is quite difficult to find works trying to deal with both modes at the same time. However, such a methodology able to work with both combustion modes is very interesting when CAI and SI combustion can coexist in the same engine, because at some given operating points, it could be really difficult to know the exact combustion process nature. The particular case of the SACI combustion (Spark Assisted Compression Ignition), also known as SICI (Spark Ignition Compression Ignition)[16], puts in evidence the need to develop analytic tools to evaluate in detail the combustion process under those conditions. As an example, Olesky et al.[17] defined a method to detect the transition between SI to CAI combustion. This was based on the change in the curvature of the heat release law just after the initial gradual heat release period (i.e. flame propagation), assuming that this change was due to the change in combustion development, as it can be seen in Figure 1.

Other authors, as Persson et al.[18], worked also to identify the instant when the combustion mode changed from SI to CAI by the pressure signal analysis, and Reuss et al.[19] worked on the identification of the cycle-to-cycle variation origins of the SACI combustion, mainly generated at the beginning of the flame kernel growth[20]. In this work they also worked on the combustion modes differentiation, basing their analysis on the pressure signals and the HRR traces.

Finally, it has to be noted that nowadays this type of works related to the combustion analysis are being replaced by detailed chemistry models and CFD simulations, since this kind of approaches allow obtaining directly many intermediate parameters that cannot be measured or obtained experimentally. With these tools, the real fuel (i.e. a blend of many different hydrocarbons) is substituted by a surrogate fuel (built from a few hydrocarbons, the chemistry of which is known), which allows the accurate combustion characterization. It is true that these methodologies are more predictive than analytical, but they are also used to look in detail the combustion performance and to compare the results with the experimental data as a way to analyze the combustion process. Around the literature it is very easy to find works about these simulations to characterize the combustion process, comparing the CFD results with experimental data[21;22]. Nevertheless, the required time and computing power make these tools sometimes unafordable, and their use is restricted to a few number of operating points.

This evolution of the combustion modes entails some doubts about the suitability of using the standard combustion diagnostics and its subsequent analysis for them, or if it should be complemented or improved. The use of SI engines combined with the implementation of lean combustion and CAI combustion modes, on the one hand, rises the importance to proceed to the combustion diagnostic cycle by cycle[23], in order to take into account the intrinsic variability of these engines and their higher combustion control complexity[24]. And, on the other hand, the standard combustion analysis methodologies present some lacks if a deeper information to distinguish the different combustion modes has to be established from the HRL information.

The purpose of this paper is to present a deeper combustion analysis methodology to study the HRL in depth in both SI and CAI modes. In this way, the differences between these two combustion modes can be studied, and the differences between a combustion sustained by a standard flame front progression and a combustion developed by autoignition can be quantified in some way.

In this document, five sections can be found: first, the current section, introduction; second, the description of the experimental tools and necessary methodologies; third, the description of the approach to study the combustion evolution from the HRL; fourth, the results obtained with
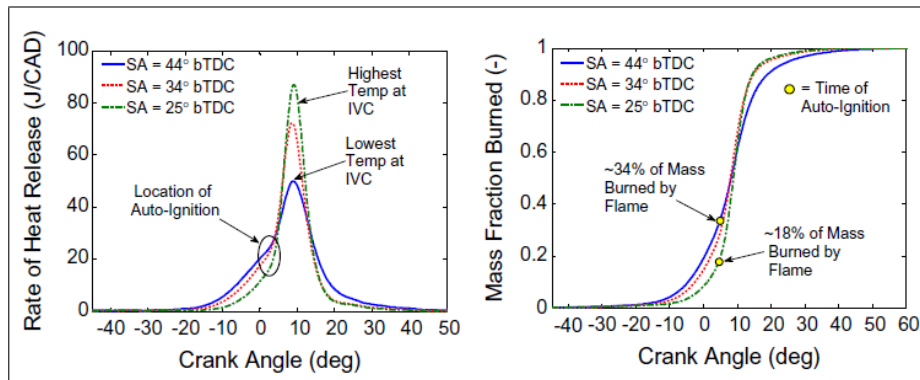
Figure 1. Left - rate of heat release. Right - Mass fraction burned curves where the change from SI to CAI combustion is marked by the yellow dots. Source: Olesky et al.[17].

the proposed methodology; and fifth, the conclusions derived from this work.

Experimental facilities and methodology

Experimental tools: the engine and the test bench

The engine used to obtain the necessary data for this work is a two stroke, single cylinder engine with approximately 0.3 liters of total displaced volume. As a brief description, this engine is a SI engine operated with gasoline, with a uniflow scavenged configuration, direct air-assisted fuel injection, and a VVT system in the exhaust camshaft. The main characteristics of the engine are given in Table 1. Some of the magnitudes in the table are given as mere approximations because of confidenciality issues. This engine was developed in the context of the ULCGE (Ultra Low Cost Gasoline Engine) project, carried out by Renault. More details about the project and the engine are available at[25].

Because of its characteristics, this engine can switch between two different combustion modes: SI and CAI. The operation in one or the other mode mainly depends on the mixture reactivity, which will allow or not the autoginition of the mixture[25]. In fact, this parameter is strongly affected by the engine load, and consequently the different combustion modes are operated as a function of the engine load, as illustrated qualitatively in Figure 2:
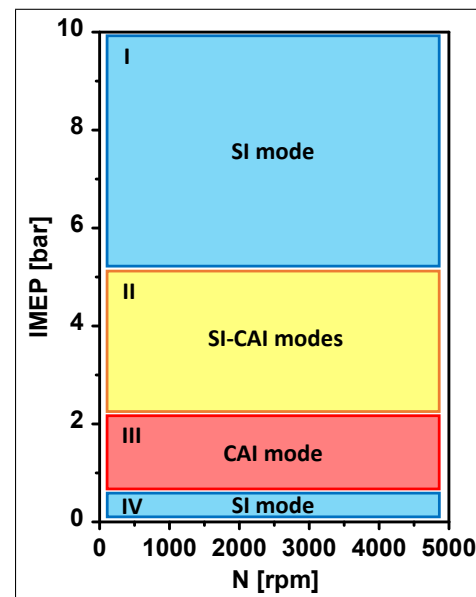

Figure 2. Definition of the different combustion regions of the engine.

- Region I: at high loads, the combustion process is controlled by the spark, as in any conventional SI engine. In this scenario, the autoignition of the mixture is dangerous for the mechanical integrity of the engine (knock), and consequently it needs to be avoided.

- Region II: at medium loads, a transition between SI and CAI takes place, and a hybrid combustion situation can appear.

- Region III: at low loads, the fuel burns in purely controlled autoignition (CAI) mode because of the enhanced reactivity of the in-cylinder charge, caused by the high amount of hot residual gases.

Displacement:	∼300 [cc]
Bore/Stroke:	∼1 [-]
Geom. compression ratio:	∼11 [-]
Valve train:	VVT (exhaust camshaft).
Fuel injection system:	Air-assisted system.
Injection pressure:	∼10 [barA] (fuel), ∼7 [barA] (air).
Intake:	Roots external compressor + cooling/heating system, to control pressure and temperature.
Exhaust:	Back-pressure electro-pneumatic valve for pressure regulation.
Fuel:	Commercial 95 RON gasoline.

Table 1. Main engine specifications.

- Region IV: there is also a small region at the lower loads, where the reactivity of the charge is not enough to support a CAI combustion process. Therefore the engine is operated in SI conditions.

Another important part related to this work is the instrumentation to measure the pressures, temperatures and amounts of the different mass flows inside the engine. For this end, different sensors are installed in the engine, in the exhaust and intake lines, as well as in the injection system:

- Two piezoelectric pressure sensors installed on the cylinder head to measure the instantaneous cylinder pressure. The reason to measure twice this signal is to detect any deviation on the pressure signals indicating a failure of the sensors, since this is the most important measurement to estimate the HRL.
- Five piezoresistive sensors at the intake, exhaust, inside the cylinder (placed close to BDC[†]), and two at the injection system.
- K-type Thermocouples installed at the intake, the exhaust, the injection system, and the inlet and outlet of the cooling and lubricating systems.
- Mass flow meters for the intake, and for the fuel and air supplied through the injection system.

The characteristics and the accuracy of the main instrumentation used in this work are summarized in Table 2. And a schematics of the engine test bench is provided in Figure 3.

Methodologies and definitions

In this paper some variables related to the combustion process and the engine operation are going to be shown. These variables are calculated or estimated as explained in the following lines:

- Definition of the operating points: the definition of the operating points will be as, for instance, XXXXrpm@YYmg, where XXXX is the engine speed in rpm and YY is the injected fuel mass per cycle in mg/stk. This nomenclature to identify the operating points will be used along the whole document. In Table 3 an overview of all the operating points used in this research is given. As indicated in the table, many operating conditions have been swept, to have a wide engine operating range.
- Knock characterization: in this study, knock is defined with the MAPO parameter (Maximum Amplitude of Pressure Oscillations)[26]. When this parameter exceeds a given limit value with a frequency higher than 0.1 Hz, knocking combustion is considered to be occurring.
- Fuel/Air equivalence ratio definition: This engine, because of being a 2S engine, is strongly affected by the trapping efficiency[27]. This leads to a difference between the equivalence ratio measured at the exhaust (Fr_{app}), and the actual equivalence ratio inside

---

[†]The information of this sensor is used for pegging the signal of the two previous piezoelectric sensors.

Magnitude	Sensor	Range	Accuracy
Temperature	Thermocouple Type K	-200:1200 ^{o}C	$\pm$ 1.1 ^{o}C or 0.4% RV
Mean pressure	Piezoresistive PMA PM40	0:6 [bar]	$\pm$ 0.3 FS
Fuel mass flow	Horiba FQ-2100DP	0.2:108 [kg/h]	$\pm$ 0.1 RV
Air mass flow	ABB Sensyflow FMP700P	1:60 [kg/h]	$\pm$ 1% RV

Table 2. Main characteristics and accuracy of the instrumentation used in the test bench (FS: Full Scale, RV: Reading Value).
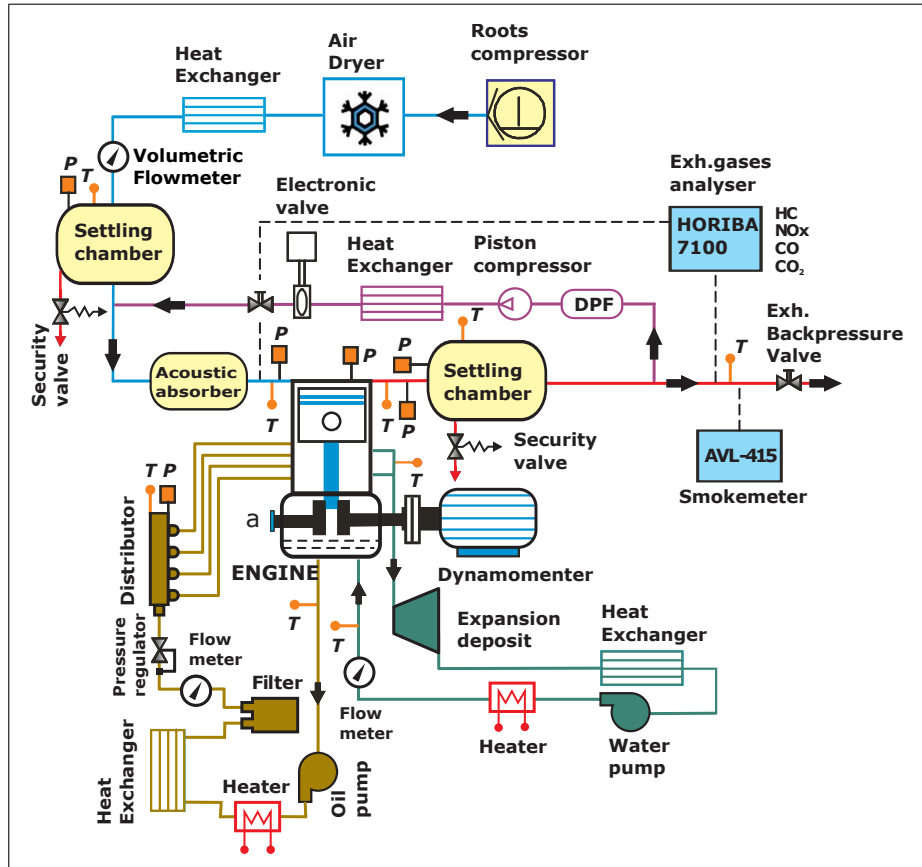

Figure 3. Schematics of the engine test bench.

the cylinder (Fr_{cyl}), since part of the fresh gases introduced can be short-circuited directly to the exhaust (this short-circuited mass depends on the operating conditions). Therefore, the considered F/A eq. ratio during the combustion is the Fr_{cyl} for the different calculations in this engine.

Finally, the most important part of this study is the chosen methodology for the HRL estimation. For this end, the HRL's are calculated by the inhouse code Calmec[28;29] using a classical procedure, which makes use of the instantaneous in-cylinder pressure, applying the first law of thermodynamics and a heat losses model based on the Woschni equation. From this model the HRR's, the combustion positions

(defined as CAXX, where XX represents the fuel mass fraction burned) and duration are obtained.

As stated in the previous lines, this HRL is going to be further analyzed, trying to remove the different effects of the fuel, the combustion conditions and others, with the aim to look for a combustion pattern, assuming that it is governed by a flame front propagation. By this way, if the "ideal flame front combustion" is characterized, the real measured combustions can be compared and studied in order to see what happened during any particular engine cycle.

All this process to go deeper into the HRL information is detailed in the next subsection. The procedure used here is inspired by the one already extensively used in constant

Magnitude	Range
Engine speed [rpm]	2000 – 4000
Fuel mass [mg/stk]	3 – 17
IMEP [bar]	1 – 9
Fr_{app}	0.5 – 1
Y_{O2}	0.1 – 0.23

Table 3. Explored engine operating conditions.

volume vessels, to characterize the laminar flame speed (as, e.g., in Metghalchi and Keck [10] and Rhodes and Keck [11]). A similar procedure has already been used in a facility closer to a real engine (an optical-accessible engine) in order to determine the turbulent flame speed, as e.g. in Afkhami et al. [30]. The main novelty of the present paper is to adapt this methodology to a real engine, able to operate in a wide range of running conditions (especially in terms of F/A ratio and exhaust gas fraction), using only the pressure trace information (without any need to have an optical access).

Results and discussion

Analysis methodology approach

In this section, the SI combustion is going to be deeper analyzed decomposing the experimental HRR's and searching for the basic evolution of the flame front at different combustion conditions. The goal of this analysis is to be able to characterize the "ideal" SI combustion for this engine, getting a valuable information to be used later for the analysis of the different combustion cycles, so as to have a deeper understanding of the different agents affecting the combustion development. Once the SI combustion details would have been studied, the CAI combustion could be also analyzed with the same approach, in order to search for the differences on the combustion evolution and, if possible, to define a methodology to differentiate both combustion modes during the experimental data processing.

Data pre-processing

Before starting with the combustion analysis proposed in this work, the necessary data has to be refined, adapted, or even recalculated in some cases, from the available measured data.

- Processing of the different individual cycles of each test

  This analysis takes each measured cycle separately, and thus the necessary initial data has to be individualized. The start of the processing methodology requires the pressure data, the calculated HRL and the mass flows of all the different gases (and fuel) inside the engine. For this purpose, the methodology shown in [23], defined to analyze the tests cycle by cycle, is used here to calculate the necessary individualized data from each test.

- HRL refinement

  The heat release laws present inaccuracies in some cases. These ones come from different origins, as disturbances on the pressure signals or deviations due to the difficulties to estimate accurately the trapped mass and the initial conditions of the cylinder charge at the beginning of the cycle. To solve some of these problems (in particular, the disturbances on the pressure signal), the pressure signal is filtered, and the effect of these disturbances is easily removed. However, the deviations in the estimated trapped mass are more complicated to be solved, and this problem worsens with the decrease in engine load, since the relative errors increase. This problem can be observed in Figure 4, where the HRL curve presents a significant

slope, both during the compression stroke, and at the end of the expansion stroke. These slopes cannot be real, and lead to wrong calculations when the HRL is processed. To solve this problem, the SOC and EOC (start and end of combustion) are defined and these slopes are removed. In this way, the HRL is correctly placed on the vertical axis. Finally, it should be noticed that all HRL's curves in this work move between 0 and 1, because they are normalized by the total heat actually released in the combustion chamber. This means that the effect of the combustion efficiency will not affect the HRL curves, thus making easier the analysis.
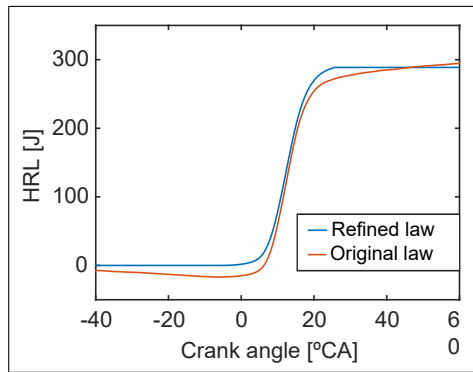

Figure 4. Original vs. processed HRL.

• Instantaneous temperatures

During the analysis of the combustion process, it is necessary to know the instantaneous conditions in the two regions of the combustion chamber (burned and unburned regions). This calculation is performed through the pressure signals and the estimated instantaneous composition of the in-cylinder charge. First, the mean in-cylinder temperature (T_{avg}) is calculated by means of the equation of state for ideal gases (Eq. 1). In this equation, p_{cyl} is the cylinder pressure, V is the instantaneous volume of the combustion chamber, R is the constant for the particular gas trapped in the cylinder (estimated from the in-cylinder composition), and m is the trapped

mass, the value of which evolves during the cycle (it changes slightly due to blow-by losses). This estimated temperature will be used later to estimate the temperatures of the burned and unburned regions during the combustion process.

$$T_{avg} = \frac{p_{cyl} \cdot V}{R \cdot m} \; [K] \qquad (1)$$

The temperature in the unburned region (T_{ub}) is considered to be equal to the average in-cylinder temperature during the period in between the IVC and the SOC, and after this point, it is estimated as an adiabatic compression process of the unburned gases caused by the expansion of the burned mass generated during the combustion process, as illustrated in Eqs. 2 and 3, where gamma is calculated with the instantaneous temperature and composition of the unburned gas.

$$\text{If } IVC < \alpha < SOC, \; T_{ub}(\alpha) = T_{avg}(\alpha) \; [K] \qquad (2)$$

$$\text{If } \alpha > SOC, \; T_{ub}(i) = T_{ub}(i-1) \cdot ...$$
$$... \frac{p_{cyl}(i)}{p_{cyl}(i-1)}^{\frac{\gamma_{cyl} - 1}{\gamma_{cyl}}} \; [K] \qquad (3)$$

Once this temperature is estimated, the density of the unburned mixture (ρ_{ub}) can be deduced, as shown in Eq. 4:

$$\rho_{ub} = \frac{p_{cyl}}{R \cdot T_{ub}} \; [kg/m^3] \qquad (4)$$

Finally the burned region temperature (T_b) is estimated, from the start of combustion, as an enthalpy balance between the unburned region temperature and the mean temperature during the combustion process, as shown in Eq. 5. The different c_p values are estimated from the composition and instantaneous temperatures for the in-cylinder charge $(c_{p_{cyl}})$ and the burnt gases $(c_{p_{exh}})$, and the HRL represents the fraction of mass burned at each instant.

$$T_b = ...$$
$$...\frac{((c_{p_{cyl}} \cdot (1 - HRL) + c_{p_{exh}} \cdot HRL) \cdot T_{avg})}{c_{p_{exh}} \cdot HRL} - ...$$
$$...\frac{((1 - HRL) \cdot T_{ub} \cdot c_{p_{cyl}})}{c_{p_{exh}} \cdot HRL} \ [K] \quad (5)$$

With all these calculations, the different temperatures and densities of the two different regions during the combustion can be estimated. An example of some of the results obtained is shown in Figure 5, where the instantaneous temperatures are illustrated.
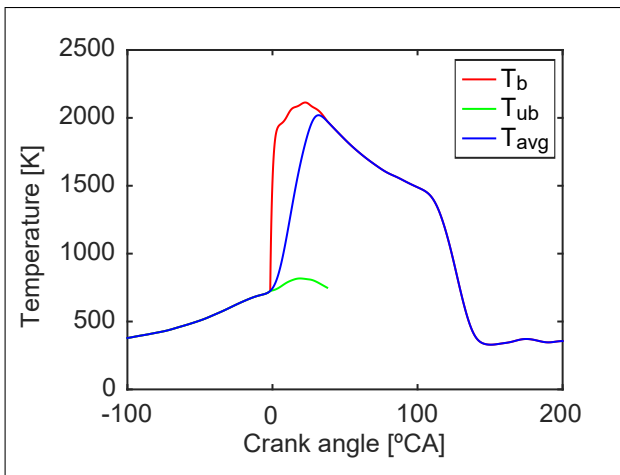

Figure 5. Example of the calculated temperatures for a high load operating point.

HRR processing

Now, once the necessary data is ready, the obtained HRR from the HRL is going to be further analyzed, decomposing it in order to subtract the different effects affecting this heat release and, thus, going deeper in the analysis of the different parameters affecting the combustion development. In this way, the resulting data of different tests performed in the engine could be compared despite having different settings.

This process can be separated in different steps, which are described below.

1st step:...
$$...HRRmf \ [g/s] = HRR \ [J/s]/LHV \ [kJ/kg] \quad (6)$$

In the first step the effect of the fuel is removed from the HRR, as shown in Eq. 6, where the HRR is divided by the Lower Heating Value (LHV) of the fuel. The result is a mass flow rate, indicative of the fuel burned at each instant (HRRmf).

2nd step:...
$$...HRRmsq \ [g/s] = HRRmf \ [g/s] \cdot ...$$
$$...(1 + (1/FstO_2 \ [-] \cdot YO_{2cyl} \ [-] \cdot Fr_{cyl} \ [-])) \quad (7)$$

With this mass flow rate of burned fuel, the mass flow rate of unburned mass (i.e. the mass flow rate going through the flame front) can be determined (HRRmsq). It is important to distinguish the HRRmf from the HRRmsq, since this last parameter takes into account the amount of gases mixed with the fuel, modifying the first parameter as a function of the in-cylinder F/A eq. ratio, the dilution of the charge (YO_{2cyl}), and the oxygen required in a stoichiometric combustion ($FstO_2$).

3rd step:...
$$...AS \ [m^3/s] = (HRRmsq/1000) \ [kg/s]/\rho_{ub} \ [kg/m^3] \quad (8)$$

If this last mass flow rate is divided by the density of the unburned mixture (ρ_{ub}), the AS parameter is obtained. This parameter is representative of the volume flow rate during the combustion. Once this value is obtained, two hypotheses can be considered in the context of turbulent premixed flames to continue with the analysis:

The first one considers the area (A) as an effective area (A_{eff}) of the flame front and the combustion speed (S) as the laminar combustion speed at those conditions (S_L). With this assumption, the effective area is the result of a "theoretical" area developed in laminar conditions (A_{geo}), i.e. a smooth surface, which is later wrinkled by the in-cylinder charge turbulence (the surface increasing factor representative of the turbulence effect is taken as k), increasing its area to make it equivalent to the flame front effective surface. Finally, this area is multiplied by the laminar combustion speed, since each differential area is assumed to progress under laminar conditions, see Eq. 9.

$$A_{eff} \cdot S_L = (A_{geo} \cdot k) \cdot S_L \qquad (9)$$

The second hypothesis considers the area (A) as the theoretical area developed in laminar conditions (A_{geo}) and the speed (S) as an equivalent speed (S_b), adding the turbulent effect to the laminar combustion speed. In this way the result is basically the same as before, even if now the turbulence effect is associated to the modification of the combustion speed, as shown in Eq. 10.

$$A_{geo} \cdot S_b = A_{geo} \cdot (k \cdot S_L) \qquad (10)$$

Finally, it is observed that both considerations lead to the same equation. In this equation, a term (k) appears, associated to the turbulence, which increases the rate of heat release. This term is often called FSR (Flame Speed Ratio),

and is related to the internal movements of the charge, which are affected by the geometry, the scavenging process and the engine speed, among others, wrinkling the surface of the flame front (or affecting the combustion speed). If the first proposed Equation 9 is considered now, when the AS parameter is divided by S_L, the resulting parameter will be A_{eff} (or subsequently, FSR·A).

4$^{\text{th}}$ step: ...

$$...FSRA\,[a.u.] = AS\,[m^3/s]/(S_L/100)\,[a.u.] \qquad (11)$$

Dividing AS by the S_L calculated at the instantaneous in-cylinder conditions (Eq. 12), the FSRA parameter is obtained, which is representative of the effective flame front area at each instant during the combustion process.

$$S_L = S_{L_{ref}} \cdot \left(\frac{T_{ub}}{T_{ref}}\right)^{1.4} \cdot \left(\frac{p}{p_{ref}}\right)^{-0.2} \cdot ...$$
$$...\left(\frac{Y_{dil}}{0.231}\right)^{1.2} \cdot e^{-\frac{1}{2}\cdot\left(\frac{Fr-1.15}{0.9}\right)^2} \quad [a.u.] \qquad (12)$$

This laminar combustion speed is calculated by means of a new correlation obtained in the frame of this research (based on the one proposed by Metghalchi[10]), which is used to approach the S_L at the same conditions as those of the experimental tests carried out in the engine. All details about how this correlation was obtained are given in Appendix A, placed at the end of the paper.

With the FSRA parameter, the effect of the different laminar combustion speeds reached depending on the charge conditions is removed. This FSRA thus represents the evolution of the effective flame front area during the combustion process ($A_{geo} \cdot k$ -see Eq. 9-). Therefore, if the

A_{geo} evolution is assumed to be equivalent[‡] for all the operating conditions and the k (turbulence parameter) is mainly dependent on the engine speed, the FSRA should aggregate, in a similar trend, the different tests if the engine speed is kept constant. In order to show this effect, in Figure 6, a Fr$_{app}$ variation at Point 2000rpm@17mg is presented, and the standard deviation between the average cycles for each test is reduced from the HRR to the FSRA in a factor of 2.35.

As seen in Figure 6, all the steps of the analysis and the graphs derived from these calculations will be represented in a graph format where the X axis is the non-dimensional HRL. In this way, cycles with different combustion durations can be represented in the same graph, and all of them will have the same start and end. Besides, this way of representing the information allows much better comparison of the different cycles (just looking at the Y axis dimension, since the X axis is the same for all of them).

5ᵗʰ step: : $A^* \, [a.u.] = FSRA \, [a.u.]/N^f \, [a.u.]$ (13)

Once the FSRA is obtained, it is important to take into account that this parameter results from the combination of the FSR (representative of the turbulence level existing inside the cylinder) and the theoretical combustion area without the wrinkling effect of the turbulence. As widely known, the turbulence intensity can be scaled with the engine speed, and according to the Borghi diagram[31], if the engine is operated in the wrinkled flames region, the influence of the engine speed is directly proportional to the turbulence intensity[32]. Therefore, the FSRA can be divided by the engine speed in order to make all the curves obtained at different engine speeds comparable among them. In order to follow the same philosophy as in the previous equation definition (Eq. 19), the parameter related to the engine speed has been defined as

N^f, where the exponent f has to be optimized following the same methodology as for the previous step. Once some tests at different engine speed have been selected, the optimization process has been carried out, and the best f value found has been $f = 1$, thus confirming that the FSR is scaled directly with the engine speed (see Figure 7).

This new parameter will be referred as A^*, and it is representative of a constant value multiplying the theoretical geometric area of the flame front ($k \cdot A_{geo}$), which, by this means, is *experimentally* obtained.

6ᵗʰ step: Definition of a standard curve

The application of the previously explained steps has led to the A^* value (in fact, curve), where the influence of the different conditions during the combustion process were intended to be removed. Now, if this parameter is calculated for a larger number of tests representative of the SI combustion mode, the average of all the obtained results should be indicative of a standard curve, representative of the SI combustion in this engine. This curve is presented in Figure 8. The shape of this curve indicates three trends during the combustion process: first, a fast increase of the theoretical surface of the flame front during the initial development of the combustion, before reaching the chamber walls; after that, once the flame front reaches the walls, A^* stagnates, and starts to decrease slowly; finally, once only the last fractions of the mixture remain in the chamber, A^* drops much faster, until the flame front reaches the end part of the unburned mixture.

For the calculation of this representative "pattern" of the SI combustion, the operating points chosen have been the same as those used to find the laminar combustion velocity

---

[‡]The geometrical area evolution is the same if the compared combustions present the same combustion phasing. If not, this evolution would be slightly different. For the present work, this difference has been neglected. At the end of the Conclusions section some indications to improve this assumption are given as a future work.
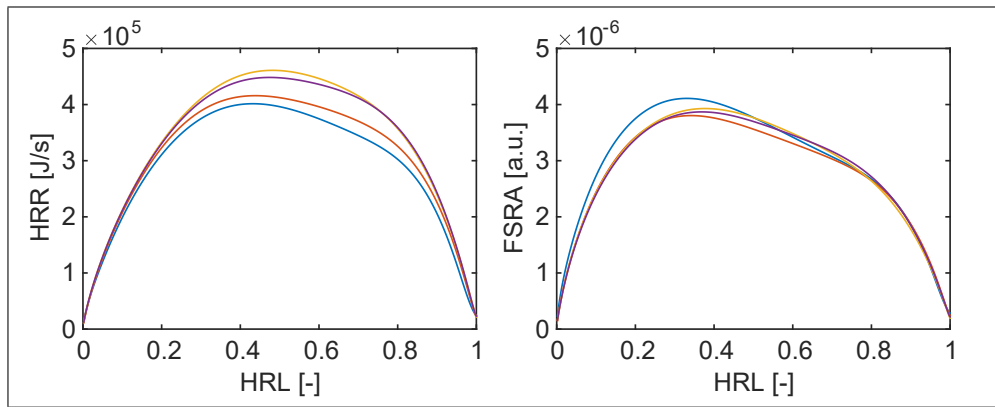
Figure 6. Comparison among the HRR and the FSRA obtained for a Fr$_{app}$ variation at Point 2000rpm@17mg.
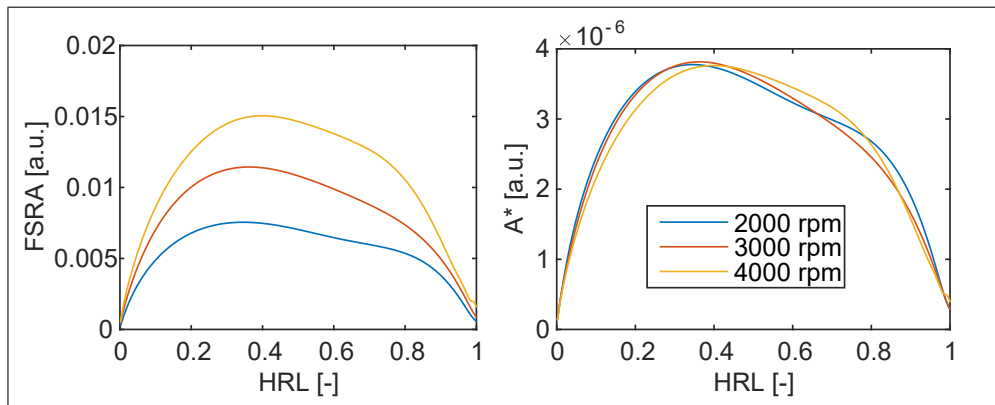

Figure 7. Correction of the engine speed. Left - FSRA values without any correction. Right - The same values corrected with f=1.
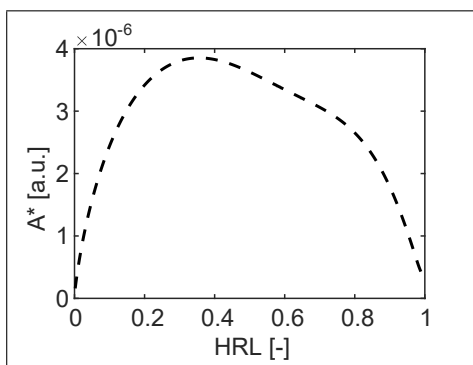

Figure 8. Representative A* value (standard curve) for the SI combustion evolution in this engine.

correlation (see Appendix A). From now on, this standard curve will be referred as "SI pattern".

7th step: Evaluation of the different operating points

Once the SI pattern and all the calculation procedure are defined, any operating point of the engine can be processed and compared with the SI pattern in order to evaluate the differences between what can be considered as an ideal SI combustion and an individual engine operation case.

Now, the way to present the results is going to be explained. Two different graphs will be presented for each case (see, e.g. Figure 9): the first graph will allow a *qualitative* comparison, whereas the second will allow a more *quantitative* comparison. The first one shows the evolution of A* against the non-dimensional HRL. Inside this graph, several plots are represented: first the SI pattern (blue dashed line) and, second, the processed operating point. Three different curves are given for the processed point: the averaged A* for the registered cycles (red continuous line), and the same curve plus and minus a standard deviation of the individual cycles (orange dashed lines). On the second graph, the quantitative difference between a given test and the SI pattern is illustrated. The

black horizontal line would represent the perfect match between both cases (Difference=0). There is also a red circle, representing the average difference between the SI pattern and the test processed (calculated as indicated in Eqs. 14 and 15; in this computation, n cycles are considered, and $A_{i,j}^*$ and $SIpattern_j$ are the vectors -as a function of HRL- representing the different curves). This Difference presents also an error bar plotted together with the red circle, which defines the standard deviation of that Difference value estimation (see Eq. 16; it is worth to note that this parameter is a standard deviation of the **average** difference of the n cycles, which justifies the n-1 term dividing the usual equation for a standard deviation). However, the value obtained for the standard deviation[§] is so small (because of the big number of cycles taken into account) that it is almost invisible compared to the ordinate axis scale of the graph.

$$Difference_i = \frac{\sum_{j=1}^{m} \dfrac{A_{i,j}^* - SIpattern_j}{SIpattern_j}}{m} \qquad (14)$$

$$Difference = \frac{\sum_{i=1}^{n} Difference_i}{n} \qquad (15)$$

$$\sigma_{Difference} = \frac{\sqrt{\dfrac{\sum_{i=1}^{n}(Difference_i - Difference)^2}{n}}}{\sqrt{n-1}} \qquad (16)$$

Now, as stated, the SI pattern will be the reference to evaluate the different tests, either if the average cycle or an individual cycle is considered. If the test shows a similar shape and scale, it would mean that the combustion has been developed as a standard SI combustion. On the contrary, if some differences are found, that will be indicative of some changes in the combustion development.

Results and discussion

The defined methodology should be capable to be used in any operating point of the engine, since the obtained SI pattern has been defined removing the effects of the load degree, the engine speed and the combustion conditions. In this subsection, the methodology will be used, first, to analyze the SI combustion on this engine for different points and conditions. After that, some CAI tests will be processed to see the results obtained by this analysis. And finally, the hybrid modes, where the combustion is developed as a combination between a SI at the beginning and changes to a CAI combustion, will be also studied with this analytical tool. This last point results very interesting, because during the combustion process, the two combustion modes have taken place, and it's very difficult to know how the process has developed.

SI conditions

For the SI conditions, some tests with different engine speeds and different Fr's are chosen. The results obtained are represented in Figure 10, showing that they fit very well with the defined SI combustion reference. The shape of the combustion evolution is very similar, and the calculated difference between the SI pattern and the tests is almost zero. These results do give a positive feedback about the analysis methodology performance, indicating that the different SI tests can be successfully processed and compared.

It is known that this engine has a high cyclic variability. Therefore, if the data is taken cycle by cycle, most of the cycles differ slightly from the average cycle, meaning that there have been slight differences in terms of combustion speed. These differences might have different origins: by the natural variability of the combustion development in SI engines caused by the ignition process and the local turbulence[33], by inaccuracies of the laminar combustion

---

[§]2σ, being representative of 68.3% of the total "population" of points of the relative difference between the two curves.
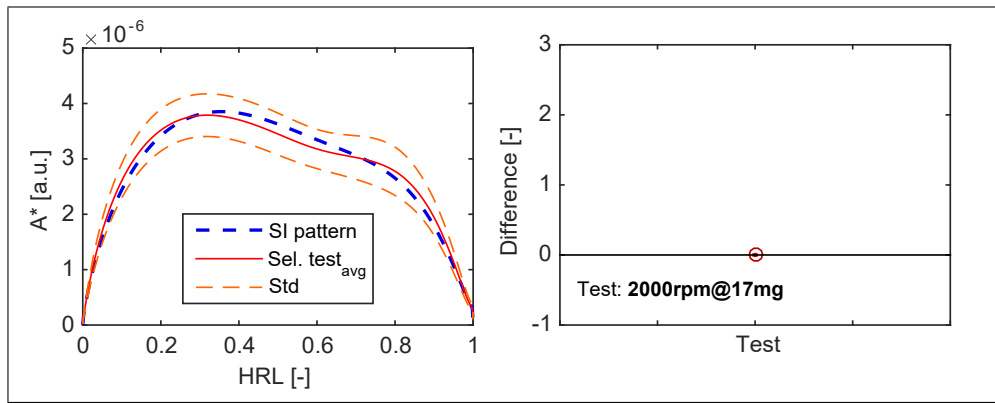
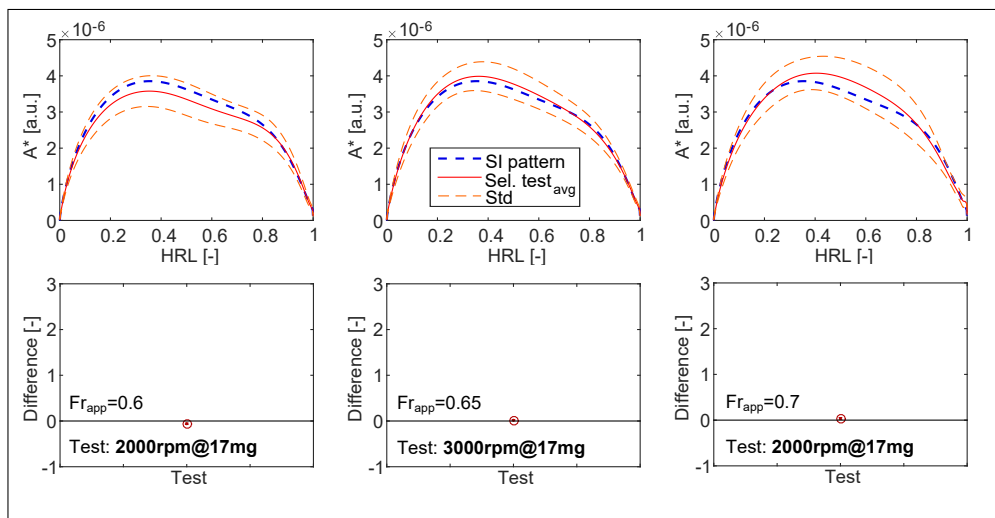**Figure 9.** Final output data for the combustion analysis.

Figure 10. Results of different SI tests processed.

speeds calculated, or due to the mixture heterogeneities during the combustion. These slight differences do not show any relevant information (at least for the present work) and are not going to be further analyzed. However, there are other cycles, more singular in shape and dimensions, that possess a relevant difference with the reference pattern. These singular cycles can be analyzed in order to understand the difference respect to the theoretical combustion that should have happened.

Figure 11 shows the A^* values of a given test at Point 2000rpm@17mg, and in a dashed black line the SI pattern. Some of the cycles of this test are going to be analyzed individually, in order to see the different situations that can be found with this combustion analysis if a SI test is processed. The chosen cycles are #60, #150 and #18, since the first one
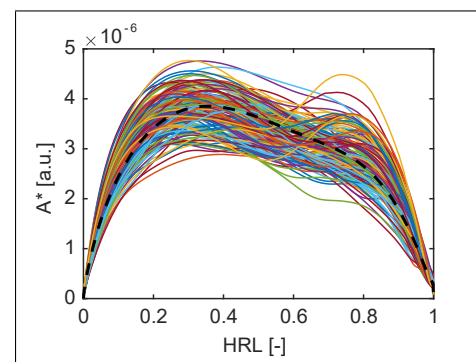

Figure 11. Representation of the A^* values for all the individual cycles in a test at Point 2000rpm@17mg.

is equivalent to the SI pattern (see Figure 12 to the left), cycle #150 presents a different shape during the last part of the HRL (see Figure 12 to the right), and cycle #18 shows the same shape, but the scale is higher (see Figure 14).

The first two cycles (#60 and #150) are plotted individually in Figure 12. Cycle #150 is out of the main

trend of the whole cycle population of this test: it presents a big increase in A* from the 60% of the heat release. If the corresponding pressure trace is examined (Figure 13), it can be said that the origin of this big increase can be associated to the knock appearance during the last stage of the combustion process. This statement is supported by the final big pressure raise and the oscillations generated after that event. Consequently, when A* starts to be higher than the SI pattern, this is because a change in terms of combustion speed has taken place, meaning that the theoretical area of the flame front has increased faster than expected. As already mentioned, this fact can be indicative of an autoignition event during the final phase of the combustion process (leading, in this case, to knock).

If these cycles are compared, the values obtained for the main combustion parameters, shown in Table 4, indicate that the combustion has been more advanced and faster in the case of cycle #150, leading to the appearance of knock, due to the high pressures and temperatures reached during the combustion process, resulting in a MAPO increment up to 2 bar.

The other cycle, #18 has been chosen because the A* values have resulted abnormally high, even though presenting the characteristic shape of the SI pattern, standing out above the other cycles. In Figure 14 this cycle is presented together with the corresponding pressure trace, and in Table 4, some values of the combustion performance can be seen. In this case, the combustion has been developed faster than the cycles shown previously, and it has been more advanced compared to cycle #60. Some knock seems to have appeared, but the value of the MAPO is still inside the acceptable limits. Therefore, this cycle has an abnormally high speed of combustion, but it is not easy to find the reason for this behavior with the available data (maybe a slight autoignition event at the beginning of the combustion process).

Based on these results, the suggested methodology has shown to be valid to fix a reference of the "normal SI combustion development", and, in this way, it is a useful tool to evaluate the different cases and identify the abnormal cases.

CAI combustion

The CAI combustion follows a different combustion pattern. Its evolution is defined by the chemical mechanisms, resulting in a faster combustion process, where there is not a single flame front consuming the unburned mixture[34–36]. These differences should be appreciated if a CAI point is processed and compared to the SI pattern. The operating Point 2000rpm@4mg has been selected as representative, because it is a stable CAI point, operated in Region III of the engine map.

The result of this analysis shows, in Figure 15, many differences respect to the SI pattern (which represents the theoretical combustion development at these conditions assuming SI operation). The most striking difference is the huge separation of the A* values from the SI reference, resulting in an equivalent theoretical surface of the flame front much higher during the combustion evolution. There is also a significant difference in shape between the two curves (the SI pattern and the average cycle): the shape is now more symmetric. The difference between the two curves calculated from all the HRL shows that the theoretical flame front surface of the CAI combustion has developed 4 times[¶] higher compared to the one corresponding to SI conditions. This means that, in this case, the combustion process has been 4 times faster, in average, because of its CAI nature.

These differences are repetitive for the different CAI operated points, no matter the load degree, the engine speed or the combustion conditions. Then, this methodology offers

---

[¶]The number 4 comes from the following reasoning: based on the figure, the relative difference $(S_{CAI} - S_{SI})/S_{SI}$ is 3. To obtain S_{CAI}/S_{SI}, the value of 1 needs to be added to the previous expression, thus being 4.
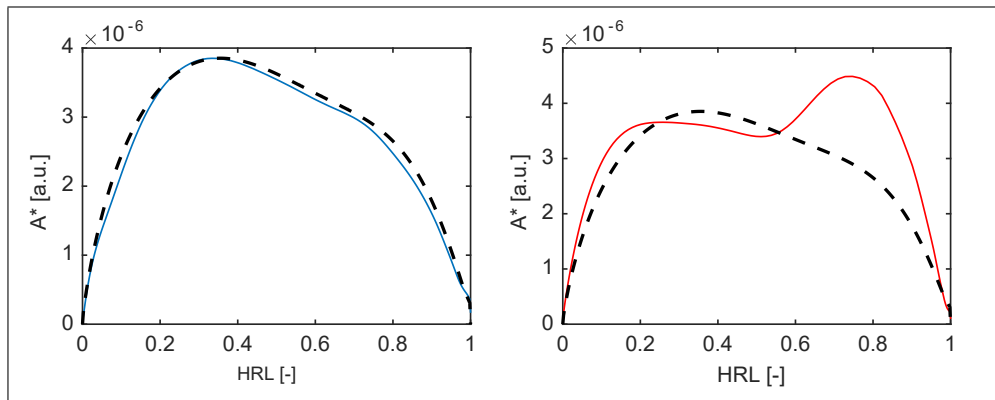
Figure 12. Representation of A* of cycles #60 (left) and #150 (right).

Data	Cycle #60	Cycle #150	Cycle #18
CA50 [ºATDC]	18.95	12.95	12.2
CA75 [ºATDC]	25.45	16.7	16.2
CA25 [ºATDC]	13.45	7.7	8.2
comb dur [ºCA]	12	9	8
MAPO [bar]	0.096	1.96	0.7621
Fr [-]	0.73	0.73	0.72

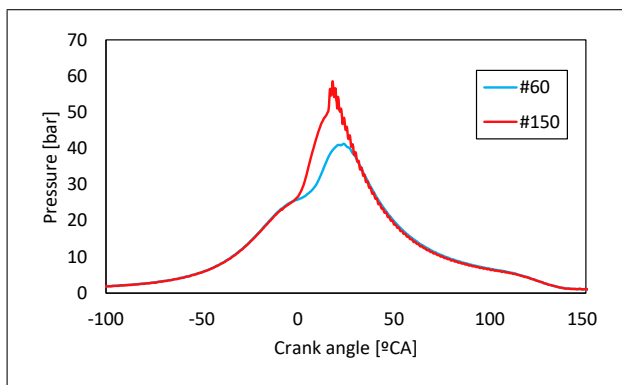**Table 4.** Different values for cycles #60, #150 and #18

Figure 13. Cylinder pressure for cycles #60 and #150.

an analytical way to differentiate CAI combustion from SI combustion. As an additional example, two other operating points (see Figure 16) have been considered, to repeat the same analysis as the one already presented previously (Figure 15). With these new points, a higher load and a lower load respect to the previous point, have been explored. In Figure 17, a summary of the effect of the engine load on the CAI to SI difference is presented. It can be seen that, as the load is decreased, the difference between CAI and SI combustion is higher, since the SI combustion for low loads results worsened due to the excessive in-cylinder charge

dilution (i.e. very low YO_2), and the lower temperatures and pressures. It can be concluded that the CAI mode enhances combustion velocity, and the lower the load, the higher the enhancement.

Hybrid modes, CAISI combustion

The combustion defined as hybrid mode combines an initial part of the combustion developed by a SI flame front with a CAI combustion that consumes the rest of the unburned mixture at the end of the combustion process. In the previous lines the results obtained of SI and CAI combustions have been analyzed, showing the different trends and values obtained for these different combustion modes. Now, it would be very interesting to see the results obtained if this hybrid combustion is analyzed, in order to see how the evolution of the combustion is performed during the cycle, and to check if both events can be differentiated. To illustrate this combustion mode and try to evaluate the combustion performance, a set of tests at Point 2000rpm@5mg have been chosen and presented in Figure 18. This set of tests is a Fr_{app} variation, starting with lean mixtures and increasing
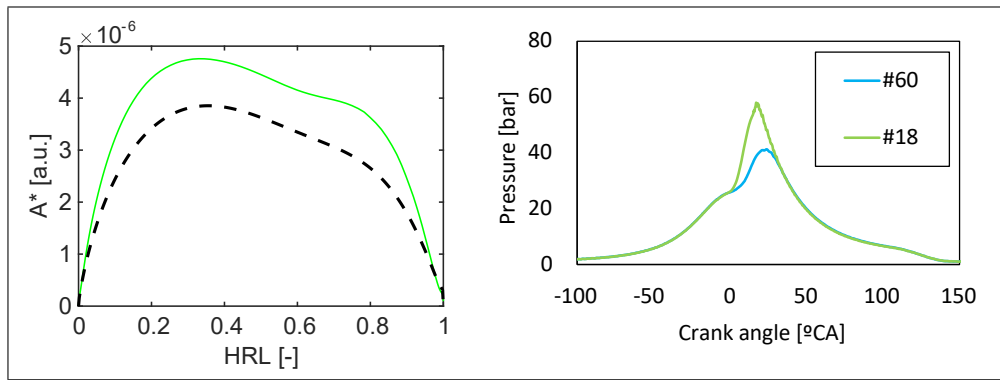
Figure 14. Representation of A* and the cylinder pressure of cycle #18.
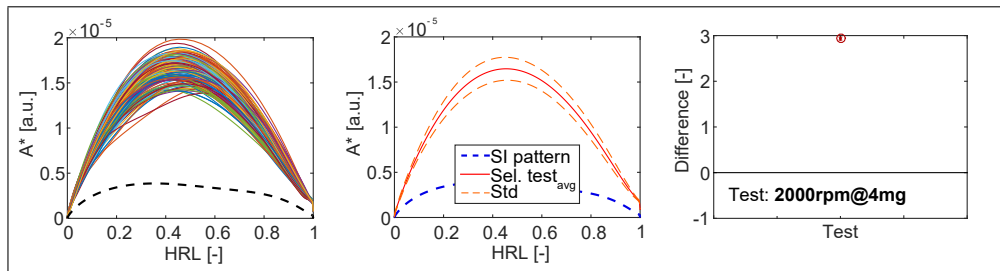

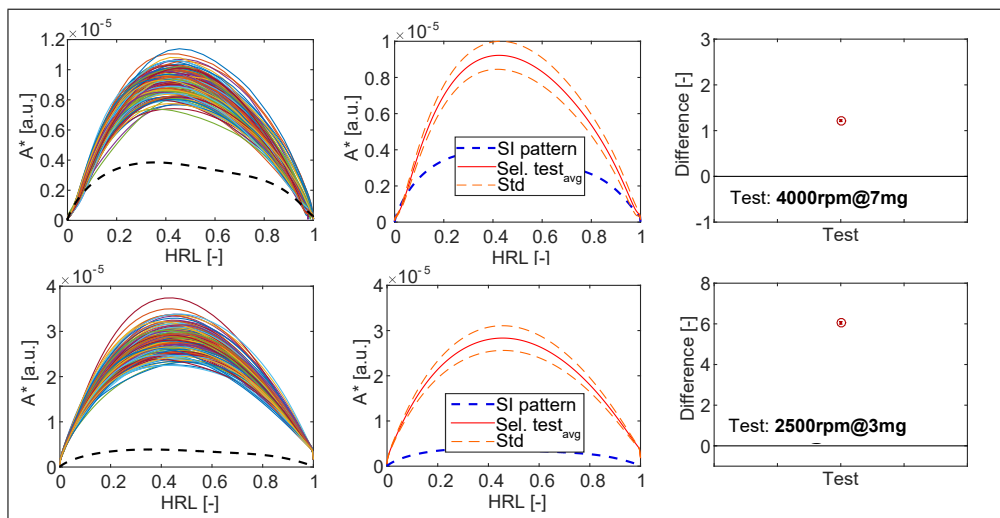**Figure 15.** Combustion analysis of Point 2000rpm@4mg operated in CAI conditions.

Figure 16. Combustion analysis of Points 4000rpm@7mg (above) and 2500rpm@3mg (below) operated in CAI conditions.

Fr progressively. By this means, the combustion starts being operated as SI to finish the tests as a CAI operated point.

The leaner Fr was expected to be a SI combustion test. This one shows a start of combustion very similar to the SI pattern, but from ~30% of the combustion process on, the A* values start to increase faster than the SI pattern, meaning that from that moment, part of the mixture has autoignited. Consequently, this point can be considered to burn under a hybrid combustion mode. In this particular case the transition to CAI conditions takes place relatively late, and a significant part of the mixture is burnt under SI conditions. As Fr is increased, if attention is paid to the Fr_{app}=0.7 case, the combustion process starts being very similar to the SI pattern, but from a very early HRL value (10% approx.), the A* value starts to increase very fast, acquiring the CAI combustion characteristics. This is probably the most interesting point of
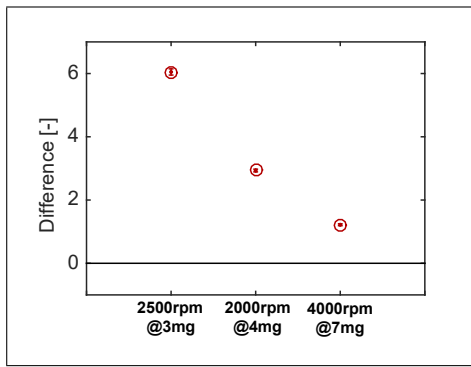
Figure 17. Evolution of the Difference parameter with the load increase.

the hybrid combustions, since the start of the combustion has been governed by the spark, and it is indeed a SI combustion, but very early it has changed to a CAI combustion.

The two other tests with higher Fr values are CAI combustion, losing the influence of the spark and therefore the control on the combustion onset. In Figure 19, the value of the calculated Difference is plotted for all these tests. It can be seen how the combustion development is changing steadily and getting more CAI.

The results obtained with this methodology have shown to be very useful to characterize the hybrid combustion modes. As expected, the SI part of the combustion follows the SI pattern, and when the combustion is changed to CAI, the A^* value indicates this change moving beyond the SI pattern. This makes possible the differentiation of the two combustion events and the characterization of the combustion transition during the cycle.

Conclusions

Through this paper, a methodology to analyze the HRR has been defined to get more detailed information of the combustion development when the engine is operated. This work has offered the results summarized in the following lines.

An adapted new correlation for the laminar combustion speed for the engine has been defined. This correlation has allowed to better characterize the effect of the F/A

equivalence ratios and the YO_2 on the combustion velocity. The results have shown that it is a more suitable S_L correlation compared to some other correlations taken from the literature. But it has to be noted that this correlation is specifically adapted for this particular engine, because of the way it has been obtained: the exponents of the different terms in the correlation were searched trying to minimize the dispersion of the different A^* curves, aiming at finding a SI combustion pattern for this particular engine. To use it in other engines, most probably the exponents have to be adapted accordingly.

The methodology has shown to be valid to define a standard SI combustion for different conditions, and compare it to the experimental data to get info about the combustion performance, to identify irregularities during the combustion, and to detect anomalous cycles. Taking this SI reference, the CAI combustion can be processed, and therefore the differentiation between both modes can be performed. The results have shown that the CAI cycles present higher A^* values during all the combustion development, as well as a different shape compared to the SI pattern, allowing to differentiate them. This tool has also shown to be very useful in the case of CAISI tests, since the combustion process can be characterized, indicating the instant and/or the burned mass fraction when the combustion changes from SI to CAI.

However, some limitations of this methodology have been identified:

- The inaccuracies at low loads to estimate the exact Fr's and mass flows for each individual cycle lead to deviations in the results that are difficult to solve just with the corrections proposed in this research.
- The effect of the piston position affecting the geometry of the combustion chamber, and therefore the evolution of the flame front, is not considered. This additional improvement (as discussed later) could help
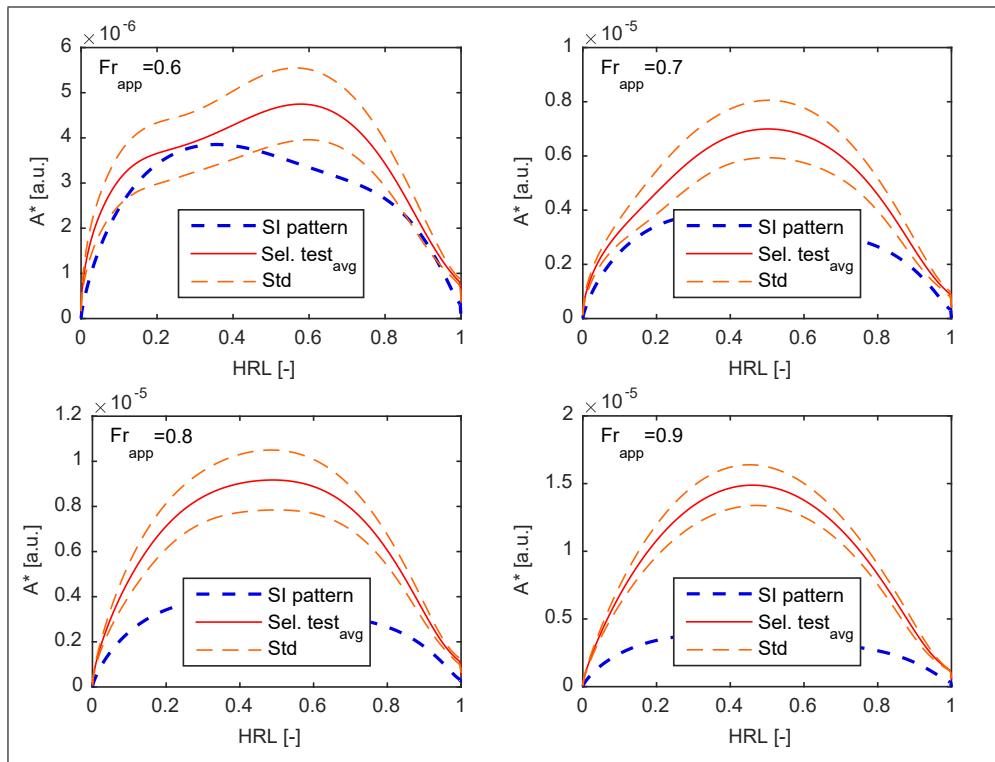
Figure 18. Results of the combustion analysis for a Fr_{app} swept at Point 2000rpm@5mg.
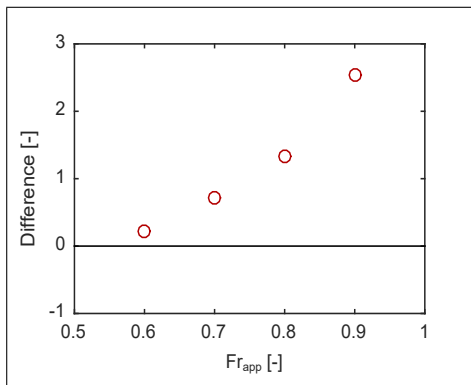

Figure 19. Difference between the SI pattern and the different processed tests of the Fr_{app} swept at Point 2000rpm@5mg.

to homogenize the different tests in a better way, and get even higher quality information.

- Another limiting factor is the competition of this method with another based on CFD. This other tool is much more complex, precise and offer a high amount of information. But it needs much more processing capacity and time. So, each tool should be used for different purposes: the tool proposed here is recommended when a lot of data needs to be analyzed, and not much time is available; whereas CFD is

probably more suitable when few data needs to be analyzed, and a lot of time is available for the analysis.

Finally some suggestions to continue with the research will be provided:

- In the current approach, A^* is considered to depend only on the combustion evolution phase (HRL, which moves from 0 to 1). This implies that the flame front area is considered to depend mainly of the distance between the flame front and the spark plug (where the flame front comes from). This hypothesis is true provided that the piston position is always the same (or, to be more specific, if the piston position evolution is the same in all cases, which means that the HRL vs. the crank angle is the same). This is quite a reasonable assumption if the combustion phasing is the same in all cases. But otherwise, A^* should be considered to also depend on the crank angle (besides that on the HRL). To make the methodology proposed in this paper

more general, this other dependency of A* would be
explored and included.

- With the current SI combustion pattern (eventually
  improved with the dependency indicated in the previ-
  ous item), a predictive SI combustion model could be
  proposed, which would have the strong advantage of
  being based on the empirical determination of A*.

Acknowledgements

Notation

Nomenclature

α	Angle
γ	Heat capacity ratio or adiabatic index
ρ	Density
σ	Standard deviation
A	Area
c_p	Specific heat capacity at constant pressure
F/A	Fuel/Air
Fr	Fuel/Air equivalence Ratio
$FstO_2$	Oxygen required in a stoichiometric combustion
m	Mass
N	Engine speed
p	Pressure
R	Universal gas constant
S	Speed

T	Temperature
V	Volume
Y	Mass fraction
Y_{dil}	Mixture dilution

Subscripts

app	Apparent
avg	Averaged
b	Burned
cyl	In-cylinder
eff	Effective
exh	Exhaust
geo	Geometric
L	Laminar
ref	Reference
ub	Unburned

Abbreviations

2S	Two Stroke
A*	Representative of the theoretical flame front area without the wrinkling effect of the turbulence
AS	Representative of the volume flow rate consumed during combustion
ATDC	After Top Dead Center
BDC	Bottom Dead Center
BTDC	Before Top Dead Center
CAXX	Crank Angle where XX% of the fuel mass has been burned
CAI	Controlled Auto-Ignition
CFD	Computational Fluid Dynamics
EOC	End Of Combustion
FS	Full Scale
FSR	Flame Speed Ratio
FSRA	Representative of the effective flame front area
HRL	Heat Release Law
HRR	Heat Release Rate

HRRmf	Representative of the fuel mass flow rate consumed
HRRmsq	Representative of the unburned mass flow rate consumed
IGR	Internal Gas Recirculation (i.e. residual gases)
LHV	Low Heating Value
IMEP	Indicated Mean Effective Pressure
IVC	Intake Valve Closing
MAPO	Maximum Amplitude of Pressure Oscillations
RV	Reading Value
SACI	Spark Assisted Compression Ignition
SI	Spark Ignited
SOC	Start Of Combustion
VVA	Variable Valve Actuation
VVT	Variable Valve Timing

Appendix A: Experimental characterization of the laminar combustion velocity

For the step #4, defined in the main text, it is necessary to define how to determine the laminar combustion speed as a function of the instantaneous in-cylinder conditions during the engine operation. If the literature is reviewed, Metghalchi and Keck[10] worked on the definition of the laminar combustion speeds for methanol, isooctane and indolene at different pressures and temperatures (Eq. 17). These combustion speeds are based on the correction of a known value of S_L for some given conditions taken as a reference. Later, Rhodes and Keck[11] defined an improved correlation for the standard gasoline, basing their work on the equation already proposed by Metghalchi.

$$S_L = S_{L_{ref}} \cdot (T_{ub}/T_{ref})^{k1} \cdot (p/p_{ref})^{k2} \ [cm/s] \quad (17)$$

where k1 and k2 are defined for each fuel, and depend on the F/A equivalence ratio[10;11].

This equation was expanded in order to take into account the addition of residual gases to the in-cylinder charge[10]. For this purpose, an extra term related to the mixture dilution was added, as illustrated in Eq. 18.

$$S_L = S_{L_{ref}} \cdot (T_{ub}/T_{ref})^{k1} \cdot (p/p_{ref})^{k2} \cdot ...$$
$$...(1 - 2.1 \cdot Y_{dil}) \ [cm/s] \quad (18)$$

This equation is reliable as long as the combustion conditions are within the defined range of use. To obtain the above equation, a relatively narrow range of F/A equivalence ratios was used. Consequently, the Fr valid range for the equation is very close to the stoichiometric conditions, and the values obtained when the calculation is out of this range are not reliable at all. The operating range of this engine, as already seen before, always present a significantly high dilution degree of the mixture, either with air (lean mixtures) or with residual gases (IGR or EGR). Therefore, knowing the limitations of the formulations proposed by Metghalchi and Keck, in the present work an alternative formulation for the laminar combustion speed estimation is going to be obtained and proposed, specifically adapted to this engine. The proposal is the following:

$$S_L = S_{L_{ref}} \cdot \left(\frac{T_{ub}}{T_{ref}}\right)^a \cdot \left(\frac{p}{p_{ref}}\right)^b \cdot ...$$
$$... \left(\frac{Y_{dil}}{0.231}\right)^c \cdot e^{-\frac{1}{2} \cdot \left(\frac{Fr - m}{d}\right)^2} \ [cm/s] \quad (19)$$

As it can be observed, the proposed equation is based on the one already proposed by Metghalchi. It depends on a predefined combustion speed value at some given conditions

taken as a reference. From this point, the combustion speed will be modified according to the current temperature, pressure, oxygen concentration and F/A equivalence ratio. However, in Eq. 19, the effect of each parameter is isolated from the others, i.e. each term in the equation depends on only one parameter (the exponents a and b, for instance, now are constants, and do not depend on Fr, as proposed by Metghalchi). Besides, the function considered for each parameter is defined based on its already known theoretical influence over the combustion speed (see Figure 20). The selection/definition of each function is justified in the following paragraph.

The functions for temperature and pressure are essentially the same as those proposed by Metghalchi, only modifying the exponent: now they are constant, whereas Metghalchi proposed a function of Fr. The major modifications in the proposed equation concern the effect of Fr and Y_{dil}, with the intention to make more flexible, reliable and "physical" their effect. The influence of the mixture dilution with residual gases has been defined as a power law of the oxygen mass fraction (YO_2), relative to the atmospheric oxygen content. In this case, the choice of the exponent determines the final influence of YO_2 on the combustion speed. It is worth noting that the function proposed here to take into account the effect of YO_2 is more suitable than that originally introduced by Metghalchi (Eq. 18), as illustrated in the bottom-left plot in Figure 20, where this last function provides negative values for oxygen mass fractions below 0.12. Finally, the Fr influence has been defined as a Gaussian function. This bell-shape function has been considered because of its consistency with experimental observations (e.g. Heywood [1]). The position of the maximum, as well as the width of the "bell" can be adjusted with the constants m and d, respectively. All the constants that need to be determined in Eq. 19 will be fitted based on experimental data taken from the engine used for this research. Details

about the fitting methodology will be given in the following paragraphs.

Regarding the reference values appearing in the equation, the following choices have been done: for the $S_{L_{ref}}$, a unitary value will be considered, and for p_{ref} and T_{ref} 298 K and 1 bar, respectively. This means that the correlation of the laminar combustion speed will not provide any physical value in *absolute* terms. Nevertheless, since the interest of this equation at this stage of the analysis is to evaluate the *relative* deviation between the different processed tests, the choice of an arbitrary value for $S_{L_{ref}}$ does not introduce any particular effect, because it is a constant value for all the considered cases. Therefore, if all the data used for the comparison is processed with the same methodology and the same fuel, there won't be any particular problem during this comparison.

The methodology to determine the different parameters of the equation proposed for the S_L calculation (i.e. the constants a, b, c, d, and m) is based on the analysis and optimization of a given group of tests, carefully selected, that are considered to have been totally burnt by a flame front (with this engine this is a very important and critical point, since total or partial CAI combustion can be found in some operating regions). The chosen points are mainly high load operating points (Region I), because in those conditions it's impossible to operate the engine by autoignition, and if this phenomenon occurs, it will be easily detected, since knock will appear. Besides, in this first phase of the analysis, the different tests have been chosen with the same engine speed and a similar load degree, to ensure that the FSR value should be equivalent for all of them. Once an appropriate group of tests at different conditions of Fr and YO_2 has been selected, the equation is tested for multiple combinations of the parameters. In each iteration, a combination is chosen and applied to calculate the different laminar combustion speeds, and with that, the FSRA values are calculated for each cycle of the selected tests (as indicated in Eq. 11). After
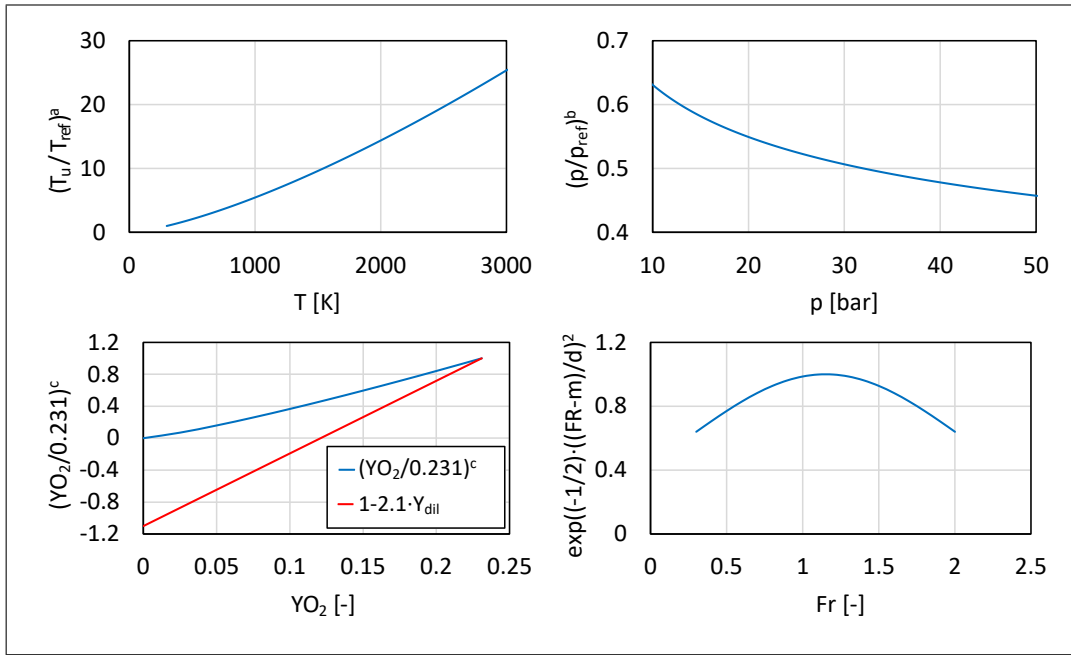
Figure 20. Functions for each parameter of the combustion speed equation.

that, the dispersion among them is calculated as the standard deviation of all the cycles respect to the mean FSRA cycle.

The optimum parameters are assumed to be those presenting the minimum dispersion on all the calculated FSRA, since this would mean that the effect of the different combustion conditions affecting the combustion speed have been satisfactorily removed from the FSRA parameter, and a "combustion pattern" would really be obtained.

Finally, after the optimization work, the parameters and the final laminar combustion speed equation for this engine are presented:

$$a = 1.4;\ b = -0.2;\ c = 1.2;\ d = 0.9;\ m = 1.15$$

$$S_L = S_{L_{ref}} \cdot \left(\frac{T_{ub}}{T_{ref}}\right)^{1.4} \cdot \left(\frac{p}{p_{ref}}\right)^{-0.2} \cdot \ ...$$

$$... \left(\frac{Y_{dil}}{0.231}\right)^{1.2} \cdot e^{-\frac{1}{2} \cdot \left(\frac{Fr - 1.15}{0.9}\right)^2} \quad [a.u.] \quad (20)$$

Once reached this point, it is worth to compare the results of the methodology proposed up to now for three different correlations for the laminar flame speed: the

correlation for isooctane presented by Metghalchi, the correlation for common gasoline presented by Rhodes, and the correlation obtained in the frame of the current research. To perform this comparison, a selection of 14 tests with their corresponding 250 cycles has been used. This selection includes information of different engine speeds, a variation of the apparent Fr between 0.5 and 1, and some tests operated with EGR up to a rate of 20%.

The result of this comparison can be observed in Figure 21, where the values for the standard deviation were σ=1.8161 for the isooctane correlation, σ=0.3578 for the gasoline correlation and σ=0.1405 for the correlation adapted to this engine. These values show that the isooctane correlation is far from being reliable in these conditions. Regarding the gasoline correlation, it is more reliable than the previous one, but when it is compared to the correlation proposed in the current work, the scattering of the curves is still 2.5 times higher. Consequently, the proposed correlation, which was specifically adapted to this particular engine, provides the best results, as expected.
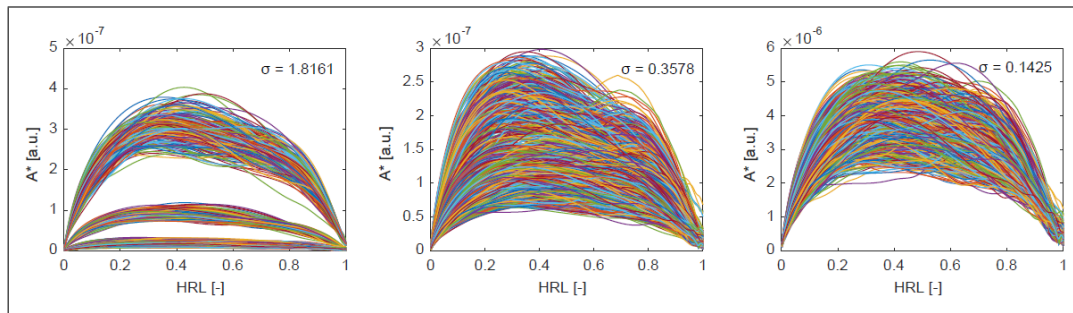
Figure 21. Representation of the A^* calculation for the three correlations of the laminar combustion speed, from left to right: isooctane correlation, gasoline correlation and proposed correlation.

References

1. Heywood J. Internal combustion engine fundamentals. McGraw-Hill; 1988.

2. Brunt MFJ, Rai H, Emtage AL. The calculation of heat release energy from engine cylinder pressure data. SAE Technical Paper n 981052. 1998;.

3. Rassweiler GM, Withrow L. Motion pictures of engine flames correlated with pressure cards. SAE Technical Paper n 380139. 1938;.

4. Gatowski JA, Balles EN, Chun KM, Nelson FE, Ekchian JA, Heywood JB. Heat release analysis of engine pressure data. SAE Technical Paper n 841359. 1984;.

5. Eriksson L. Requirements for and a systematic method for identifying heat-release model parameters. SAE Technical Paper n 980626. 1998;.

6. Egnell R. Combustion diagnostics by means of multizone heat release analysis and NO calculation. SAE Technical Paper n 981424. 1998;.

7. Ghojel J, Honnery D. Heat release model for the combustion of diesel oil emulsions in DI diesel engines. Applied Thermal Engineering. 2005;25(14-15):2072–2085.

8. Alkidas AC. Combustion advancements in gasoline engines. Energy Conversion and Management. 2007;48(11):2751 – 2761.

9. Peters N. Laminar flamelet concepts in turbulent combustion. Symposium (International) on Combustion. 1988;21(1):1231–1250.

10. Metghalchi M, Keck JC. Burning velocities of mixtures of air with methanol, isooctane, and indolene at high pressure and temperature. Combustion and Flame. 1982;48(C):191–210.

11. Rhodes DB, Keck JC. Laminar burning speed measurements of indolene-air-diluent mixtures at high pressures and temperatures. SAE Technical Paper n 850047. 1985;.

12. Gomez AJ, Reinke PE. Lean burn: A review of incentives, methods, and tradeoffs. SAE Technical Paper n 880291. 1988;.

13. Yu H, Su W. Numerical study on the approach for super-high thermal efficiency in a gasoline homogeneous charge compression ignition lean-burn engine. International Journal of Engine Research. 2020;0(0):1468087419889248. Available from: https://doi.org/10.1177/1468087419889248.

14. Lavy J, Dabadie JC, Angelberger C, Duret P, Willand J, Juretzka A, et al. Innovative ultra-low NOx controlled auto-ignition combustion process for gasoline engines: The 4-SPACE project. SAE Technical Paper n 2000-01-1837. 2000;.

15. Yildiz M, Çeper BA. Combustion development in a gasoline-fueled spark ignition-controlled auto-ignition engine operated at different spark timings and intake air temperatures. International Journal of Engine Research. 0;0(0):1468087419894165. Available from: https://doi.org/10.1177/1468087419894165.

16. Strozzi C, Claverie A, Prevost V, Sotton J, Bellenoue M. HCCI and SICI combustion modes analysis with simultaneous PLIF imaging of formaldehyde and high-speed chemiluminescence in a rapid compression machine. Combustion and Flame. 2019;202:58–77.

17. Olesky LM, Martz JB, Lavoie GA, Vavra J, Assanis DN, Babajimopoulos A. The effects of spark timing, unburned gas temperature, and negative valve overlap on the rates of stoichiometric spark assisted compression ignition combustion. Applied Energy. 2013;105:407–417.

18. Persson H, Hultqvist A, Johansson B, Remón A. Investigation of the early flame development in spark assisted HCCI combustion using high speed chemiluminescence imaging. SAE Technical Paper n 2007-01-0212. 2007;.

19. Reuss DL, Kuo TW, Silvas G, Natarajan V, Sick V. Experimental metrics for identifying origins of combustion variability during spark-assisted compression ignition. International Journal of Engine Research. 2008;9(5):409–434.

20. Sjerić M, Kozarac D, Tatschl R. Modelling of early flame kernel growth towards a better understanding of cyclic combustion variability in SI engines. Energy Conversion and Management. 2015;103:895 – 909.

21. Coskun G, Delil Y, Demir U. Analysis of an HCCI engine combustion using toluene reference fuel for different equivalence ratios - Comparison of experimental results with CFD and SRM simulations. Fuel. 2019;p. 217–227.

22. Turkcan A, Ozsezen AN, Canakci M, Coskun G, Soyhan HS, Demir U. An experimental and modeling study to investigate effects of two-stage direct injection variations on HCCI combustion. Combustion Science and Technology. 2015;187(4):642–658.

23. López JJ, Molina S, Valero-Marco J, Coma G. Influence of the analysis methodology on the combustion study in engines with high cycle-to-cycle variability. 15th EAEC European Automotive Congress, Madrid (Spain) 3-5 October. 2017;.

24. Pla B, la Morena JD, Bares P, Jiménez I. Cycle-to-cycle combustion variability modelling in spark ignited engines for control purposes. International Journal of Engine Research. 0;0(0):1468087419885754. Available from: https://doi.org/10.1177/1468087419885754.

25. López JJ, Molina S, García A, Valero-Marco J, Justet F. Analysis of the potential of a new automotive two-stroke gasoline engine able to operate in spark ignition and controlled autoignition combustion modes. Applied Thermal Engineering. 2017;126:834–847.

26. Zhen X, Wang Y, Xu S, Zhu Y, Tao C, Xu T, et al. The engine knock analysis - An overview. Applied Energy. 2012;92:628–636.

27. Benajes J, Novella R, De Lima D, Tribotté P, Quechon N, Obernesser P, et al. Analysis of the combustion process, pollutant emissions and efficiency of an innovative 2-stroke HSDI engine designed for automotive applications. Applied Thermal Engineering. 2013;58(1-2):181–193.

28. Lapuerta M, Armas O, Hernandez JJ. Diagnosis of DI Diesel combustion from in-cylinder pressure signal by estimation of mean thermodynamic properties of the gas. Applied Thermal Engineering, Vol19 no5, pp513-529. 1999;.

29. Lapuerta M, Armas O, Bermúdez V. Sensitivity of diesel engine thermodynamic cycle calculation to measurement errors and estimated parameters. Applied Thermal Engineering. 2000;20(9):843–861.

30. Afkhami B, Wang Y, Miers SA, Naber JD. Experimental determination of flame speed and flame stretch using an optically accessible, spark-ignition engine. International Journal of Engine Research. 0;0(0):1468087419877718. Available from: https://doi.org/10.1177/1468087419877718.

31. Pairy F, Desantes JM. Motores de combustión interna alternativos. Editorial Reverté and Editorial UPV; 2011.

32. Bopp S, Vafidis C, Whitelaw JH. The effect of engine speed on the TDC flowfield in a motored reciprocating engine. SAE Technical Paper n 860023. 1986;.

33. Vermorel O, Richard S, Colin O, Angelberger C, Benkenida A, Veynante D. Towards the understanding of cyclic variability in a spark ignited engine using multi-cycle LES. Combustion and Flame. 2009;156(8):1525–1541.

34. Zhao H, Li J, Ma T, Ladommatos N. Performance and analysis of a 4-stroke multi-cylinder gasoline engine with CAI

combustion. SAE Technical Paper n 2002-01-0420. 2002;.

35. Xie H, Li L, Chen T, Zhao H. Investigation on gasoline homogeneous charge compression ignition (HCCI) combustion implemented by residual gas trapping combined with intake preheating through waste heat recovery. Energy Conversion and Management. 2014;86:8 – 19.

36. Zhang Y, Zhao H. Investigation of combustion, performance and emission characteristics of 2-stroke and 4-stroke spark ignition and CAI/HCCI operations in a DI gasoline. Applied Energy. 2014;130:244–255.